INTERNATIONAL JOURNAL OF ROBUST AND NONLINEAR CONTROL
Int. J. Robust Nonlinear Control 2002; **00**:1–6 *Prepared using* rncauth.cls *[Version: 2002/11/11 v1.00]*

Piecewise affine approximations of fluxes and enzyme kinetics from *in vivo* ^{13}C labeling experiments†

Alessandro Abate[1]*, Robert C. Hillen[1], S. Aljoscha Wahl[2]

[1] *Delft Center for Systems and Control,*
[2] *Department of Biotechnology, Kluyver Centre for Genomics of Industrial Fermentation*
TU Delft - Delft University of Technology — Delft, The Netherlands

SUMMARY

Owing to the ever increasing amount of available information on metabolic networks, and in particular to the increase in information content from *in vivo* ^{13}C dynamic labeling experiments, this work investigates the problem of reconstructing dynamic fluxes and enzyme kinetics. The model structure is based on the use of piecewise affine approximations. The optimization procedure at the basis of the model identification is improved by separating the parameter estimation procedure into two different phases. As a first step, a dynamic flux profile in time is reconstructed using functions that are piecewise affine (in time). To achieve scalability for this step, several approaches have been developed and compared. Afterwards, the time-dependent profiles are embedded in the concentration space and the enzyme kinetic functions for single reactions are identified independently. This is an advantage compared to standard complete kinetic network approaches, which are typically characterized by hundreds of parameters, since now only a few need to be optimized simultaneously. Additionally, different kinetic formats can be rapidly compared. The overall approach is demonstrated using an informative in silico experiment.

KEY WORDS: Enzyme Kinetics, Dynamic ^{13}C Labeling, Metabolic Networks, Flux Analysis, Systems Biology, Piecewise Affine Models, Model Identification

1. INTRODUCTION

Biological production processes are based on sustainable resources and are expected to replace chemical, petroleum-based production processes [1–3]. To be competitive, product yields and rates of biological systems have to be optimized [4]. In the past, various successful bio-processes based on renewable carbon sources have been commercialized, such as 1,3-Propanediol [5], Isoprene [6], and Lysine [7]. Most of these processes have gone through long development cycles, especially when the design of an appropriate microorganism (cell factory) was concerned. To

*Correspondence to: Delft Center for Systems and Control (3mE), Mekelweg 2, 2628CD Delft, The Netherlands. Phone: +31-15-27-85606. Emails: a.abate@tudelft.nl (A. Abate), s.a.wahl@tudelft.nl (S.A. Wahl).
†Work supported by the European Commission under Marie Curie grant MANTRAS 249295 and STREP project MoVeS FP7-ICT-2009-5 257005, and under the NoE HYCON2 FP7-ICT-2009-5 257462, by the NWO under VENI grant 016.103.020, and by the NGI Horizon project 93519023. Thanks to Sef Heijnen and to Peter Verheijen from the Biotechnology Department, Faculty of Applied Sciences, at TU Delft.

reduce strain design time and development effort, rational approaches are essential [8]. These approaches are formal and thus depend on precise models of metabolic, transcriptomic and genetic networks [9]. In particular, to enable the prediction of metabolic states, metabolic fluxes, and production yields, enzyme kinetic models are required. The work in [10] has pioneered the identification of *in vivo* kinetic properties based on kinetic modeling and the estimation of parameters based on time-series data from cells that are excited by a substrate pulse, where the response of the metabolism is monitored by rapid sampling [11]. A series of further studies [12, 13] has made more evident that the current data availability is not sufficient for a statistically reliable parameter estimation [14], and thus further motivated the development of models from data.

To enhance the modeling of metabolic networks, four main challenges have to be tackled:

(1) *In vivo* kinetic mechanisms. Many enzymes have been studied in much detail *in vitro*, however it has been shown that their *in vivo* conditions can differ drastically [15]. In fact, physiological parameters and enzyme kinetic mechanisms are peculiar to the living cell. A variety of models with large parameter space have to be employed and tested [14, 16] in order to select proper ones fitting *in vivo* data.
(2) Data availability. Data sets, even coming from rapid sampling [11] techniques, usually contain only few observations, typically compounded with noise. The gathering of data is impaired by technological limitations or sheer experimental costs.
(3) Limited excitation. *In vivo* experiments have typically limited dynamical ranges and, besides the substrate, only a few metabolites in the network can be fully excited. Additionally the limited information content associated to time-series of metabolites concentrations leads to multiple possible outcomes for model identification problems.
(4) Computational overhead. Optimization procedures applied to large-scale kinetic models – especially when isotopomer states are included – are demanding because of size, existence of non-linearities in the flux vs. concentration dependence, and again presence of noise.

With regards to the challenges in (2) and (3) (scarceness of data with limited information content), this study leverages dynamic datasets that are enriched by ^{13}C labeling measurements. Previous studies [17–19] have shown that adding ^{13}C labeled tracers increases the information content on pool turnover and with that intracellular fluxes. This enhances the parameters estimation accuracy, particularly in the presence of exchange and parallel fluxes, or of regulatory cycles. While [17, 18] focus on positional enrichment, this work and [19] use full isotopomer labeling. Recent improvements in sampling [20, 21] and measurement procedures [22, 23] enable labeling experiments under dynamic metabolic conditions. Experiments performed with *Penicillium chrysogenum* under dynamic conditions have shown a good reproducibility of labeling enrichments [24]. In dynamic experiments it is of fundamental importance to gather information over time-dependent quantities [17, 18]: in particular the study of flux profiles in time elucidates a number of regulation mechanisms that are key for metabolic networks [19].

A modeling approach based on hybrid systems [25] is employed to address the challenges in (1) and (4). In particular, this work is based on piecewise affine (PWA) [26] models, which are a subclass of hybrid models [27]. Hybrid systems have recently been used in systems biology studies [28–32] and are worth investigating since they are prone to formal mathematical analysis [25]. PWA models are characterized by dynamics that are piecewise linear, with offset (hence, piecewise affine) over their domain of definition (see Section 2.5) and offer an alternative to other formalism for the simplification of kinetic functions [17,33,34]. Of interest to this work, there exist developed approaches and software tools to study the system identification problem

for PWA models [35, 36]. This study uses this class of models for the identification of kinetic equations from *in vivo* ^{13}C labeling experiments.

Again with focus on challenges (1) and (4) over the problem of identification of *in vivo* kinetic parameters, [37] has put forward an approach divided in data analysis and model characterization, which is distinguished from standard techniques based on metabolic network models inclusive of all (known) kinetic equations. The use of time-series concentrations (data analysis) allows first extracting a dynamic flux profile using model-free smoothing functions and linear algebra operations, then to estimate enzyme kinetic parameters in the flux vs. concentration domain (model characterization). In a later work [38], hybrid models have been employed for the reconstruction of enzyme kinetic functions – however, unlike the present work, [38] uses power laws and allows the identification of discontinuous models. Both [37, 38] work exclusively with unlabeled data. Methodologically, while our approach is similar to that in [37] in breaking the problem into two sequential parts, we use for both parts a model-based approach (indeed, based on PWA models), whereas [37] exploits a model-free approach as a first step, followed by a second step that leverages power laws approximations. The approach based on PWA approximations allows using known theory and software from the literature [25, 39] and promises to be computationally advantageous.

Recapitulating the previous discussion, the overall goal of this work is *to provide a procedure for the reconstruction of flux profiles and enzyme kinetic functions from* in vivo ^{13}C *labeling experiments, by leveraging piecewise affine models.* The procedure is broken down into two different phases. As a first step, dynamic flux profiles in time are reconstructed from *in vivo* ^{13}C labeling data using functions that are piecewise affine (also in time) (see Section 3). This step allows one to extract quantitative information over time-dependent data, thus representing a goal in itself. Afterwards, the reconstructed time-dependent profiles are embedded in the concentration space and the enzyme kinetic functions for single reactions are identified independently (see Section 4). This is an advantage compared to a whole-network approaches, typically characterized by large sets of parameters to be optimized over. The approach is demonstrated using an informative in silico experimental setup (see Section 2.4): using known reference solutions, the proposed algorithms are benchmarked in Section 5.

2. MODELING OF KINETIC METABOLIC NETWORKS

This section discusses dynamical models for metabolic networks, and PWA models are put forward as a framework for system identification based on dynamic experiments. We will work with the following variables: c denote concentrations, v fluxes, x represent isotopomer fractions (distributions), whereas y are mass isotopomers and cy are labeled concentrations.

2.1. Metabolite Concentration Balances in a Network

A metabolic reaction network consists of a set of $\mathfrak{c}$ metabolites (their concentrations is denoted by a vector $c \in (\mathbb{R}^+)^{\mathfrak{c}}$) and a related set of $\mathfrak{v}$ fluxes (denoted by a vector $v \in \mathbb{R}^{\mathfrak{v}}$) between the metabolites in pool c. The material fluxes in v depend on enzymatic reaction mechanisms (e.g. Michaelis-Menten kinetics), substrate concentrations and allosteric effectors (c), and parameters of the mechanisms (α, namely affinity constants, maximal conversion rates, etc.). The rates of change for the concentrations in c are described by balancing the in- and out-fluxes for each metabolite pool. These balances can be expressed with a stoichiometric matrix $N \in \mathbb{Z}^{\mathfrak{c}\times\mathfrak{v}}$, which relates the number of balanced metabolites to the reactions present in the network, and via the flux functions v. These fluxes depend on the metabolite concentrations

c, as well as on the physio-chemical parameters α (e.g., kinetic parameters), and on additional parameters β encompassing operational variables (e.g. substrate feed to the reactor, dilution rates, and other experimental settings – please refer to the case study in this work for an instantiation of β), as follows:

$$\frac{dc}{dt} = Nv(c, \alpha, \beta), \tag{1}$$

where $t \in \mathcal{T}$ and $\mathcal{T} = [0, T]$ denotes the time interval of interest. The metabolite concentrations are measured over a finite discrete set of $\mathfrak{m}+1$ samples $\mathcal{T}_m = \{t_0^m, t_1^m, \ldots, t_{\mathfrak{m}}^m\}, t_i^m \in \mathcal{T}$ (sample times do not have to be equidistant, in fact a samples set could also be characteristic of a single metabolite). An example network, to be discussed shortly, is presented in Figure 1.

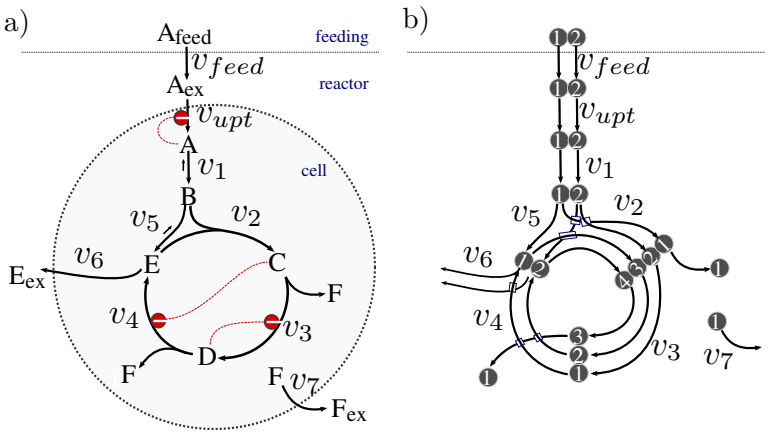

Figure 1. a) Metabolic network considered for case study presented in Section 2.4. The network presents four extracellular metabolites ($A_{feed}, A_{ex}, E_{ex}, F_{ex}$), and six intracellular ones (A to F). There are nine fluxes affecting the dynamics of the compounds, of which one feed flux (v_{feed}), three transport fluxes (v_{upt}, v_6, v_7), and the remaining being internal fluxes. b) Labeled case: atom transitions for the transfer of carbon atoms in the reaction network.

2.2. Isotopomer Balances for Labeled Networks

As an extension of the stoichiometric networks of the previous section, isotopomer networks additionally balance the isotopomer states [40], namely the state of ^{12}C- and ^{13}C-combinations in the backbone of a metabolite. For instance, glucose with six carbon atoms can provide a total of $2^6 = 64$ different isotopomer states when labeling a metabolite. In general, for each metabolite with n carbons, 2^n isotopomer states can be obtained. This significantly increases the number of (differential) equations needed to describe the network dynamics. Additionally, as will be seen shortly, the system of isotopomer balances may be non-linear [40], even if the original fluxes v are linearly related to the rate of change of the concentrations c as in (1).

In the following, the balances for two labeled pools in the example network of Fig. 1 are derived. For pool A, one in- (v_{upt}) and one out-flow (v_1) are present: the concentration of the pool c_A changes according to $dc_A/dt = v_{upt} - v_1$, where $v_1 = v_1^{\rightarrow} - v_1^{\leftarrow}$ is a bidirectional flux (as per Fig. 1). Introduce function $\iota : \{1, \ldots, \mathfrak{c}\} \to \mathbb{N}$, which associates to each metabolite (say A) the number of its carbon atoms: $\iota(A) = 2, \iota(C) = 4$. For simplicity, we may also apply function ι directly on the corresponding concentration: $\iota(A) = \iota(c_A)$. To balance isotopomer

states for metabolite A, the isotopomer distribution (or fraction) vector x_A is employed, which is composed by the isotopomer states $x_{A\#}$, where # denotes a particular labeling pattern [40]. Vector x_A has dimension equal to $2^{\iota(A)}$ and describes the fraction of the metabolite with a particular labeling pattern. The product of $x_{A\#}$ times a concentration c_A yields a labeled concentration. In the example, the labeled pool A has the following dynamics:

$$c_A \frac{dx_{A00}}{dt} = x_{A_{ex}00} v_{upt} - x_{A00} v_1^{\rightarrow} + x_{B00} v_1^{\leftarrow},$$

and similarly for the other three labeling patterns. Here $\iota(A) = 2$, and $\# \in \{00, 01, 10, 11\}$. The impact of the two fluxes on the rate of change of the isotopic state depends on the isotopic fractions for pool A_{ex}, A, and B. Notice that the labeled pool A is involved in a linear sequence of reactions, resulting in a linear set of differential equations. In case of a splitting reaction, again linear equations are obtained – for example, for labeled metabolite F, one obtains:

$$\begin{aligned} c_F \frac{dx_{F0}}{dt} &= (x_{C0000} + x_{C0001} + x_{C0010} + x_{C0011} + x_{C0100} + x_{C0101} + x_{C0110} + x_{C0111}) v_3 \\ &\quad + (x_{D000} + x_{D010} + x_{D100} + x_{D110}) v_4 - x_{F0} v_7, \\ c_F \frac{dx_{F1}}{dt} &= (x_{C1000} + x_{C1001} + x_{C1010} + x_{C1011} + x_{C1100} + x_{C1101} + x_{C1110} + x_{C1111}) v_3 \\ &\quad + (x_{D001} + x_{D011} + x_{D101} + x_{D111}) v_4 - x_{F1} v_7. \end{aligned}$$

However, this situation changes when bimolecular reactions are involved: for instance, in the case of the balances for the labeled pool C, the inflow of labeling material depends on flux v_2, but its labeling pattern hinges on two metabolites, namely B and E. To produce an unlabeled $C0000$, both B and E have to be unlabeled: the probability of this event is given by the product of the corresponding isotopomer fractions $x_{B00} x_{E00}$. The differential equations relative to the labeled metabolite C read as:

$$\begin{aligned} c_C \tfrac{dx_{C0000}}{dt} &= x_{B00} x_{E00} v_2 - x_{C0000} v_3, \\ c_C \tfrac{dx_{C0001}}{dt} &= x_{B00} x_{E01} v_2 - x_{C0001} v_3, \\ &\vdots \\ c_C \tfrac{dx_{C1111}}{dt} &= x_{B11} x_{E11} v_2 - x_{C1111} v_3. \end{aligned}$$

In general, the isotopomer balances will described shortly as:

$$D(c) \frac{dx}{dt} = g(c, x, \alpha, \beta), \tag{2}$$

which depends on (1) and where $x \in (\mathbb{R}^+)^{\sum_{j=1}^{\mathfrak{c}} 2^{\iota(c_j)}}$ represents a vector including all the isotopomer distribution vectors (one for each labeled metabolite), $D(c)$ is a diagonal matrix accounting for the metabolites concentrations (its dimension is given by the sum of the number of isotopomers fractions per each of the $\mathfrak{c}$ metabolites, $\sum_{j=1}^{\mathfrak{c}} 2^{\iota(c_j)}$), g denotes a possibly nonlinear vector function, α has the same meaning as in (1), and β additionally includes the labeled input fractions.

2.3. Measurements

Isotopomer fractions cannot be directly measured [40]. Current technologies – in particular mass spectrometry [41] and nuclear magnetic resonance [42] – allow the observation of linear combinations of isotopomers. Using mass spectrometry isotopomers are separated according

to their weight, which depends on the number of labeled carbon atoms. For metabolite C in Figure 1, five different masses can be measured: $C+0$ when no labeled carbon atom is present (this corresponds to the isotopomer state $C0000$), $C+1, C+2, C+3$ if respectively $1, 2$ or 3 carbon atoms are labeled, and finally $C+4$ in case all carbon atoms are labeled (for $C1111$). In general, a metabolite with n carbon atoms has $n+1$ (so called) mass isotopomers. The measured mass isotopomer fractions then result from a linear combination of the isotopomer fractions as follows:

$$\begin{aligned} y_{C+0}(t) &= x_{C0000}(t), \\ y_{C+1}(t) &= x_{C0001}(t) + x_{C0010}(t) + x_{C0100}(t) + x_{C1000}(t), \\ &\vdots \\ y_{C+4}(t) &= x_{C1111}(t), \end{aligned} \tag{3}$$

where $t \in \mathcal{T}_m$. From the measured mass isotopomer fractions, the measured labeled concentrations are obtained as $c_{C+r}(t) = c_C(t) y_{C+r}(t), r = 0, \ldots, \iota(C), t \in \mathcal{T}_m$, where $c_C(t)$ is the t^{th} measured sample of the unlabeled concentration of metabolite C.

2.4. Metabolic Network Case Study

The case study has been taken from [19]. The model, presented in Fig. 1, is a simplified metabolic network that recapitulates the microbial central carbon metabolism. In [19], the model has been used to analyze the impact of labeling measurements for the identification of enzyme kinetic parameters (parameters α in (1)). The model includes a linear reaction sequence (v_{upt}, v_1, v_5), a branch-point metabolite E and allosteric reaction mechanisms (on v_{upt}, v_3, v_4). The substrate A_{ex} is fed to the bioreactor by a flux v_{feed}. The mass balance for the substrate A_{ex} is $\frac{d}{dt}c_{A_{ex}} = c_{in}v_{feed} - \frac{V_{intra}}{V_{extra}}v_{upt} - c_{A_{ex}}v_{feed}$, where V_{intra}, V_{extra} are the intra- and extra-cellular volumes (denoting for the extracellular metabolite A_{ex} a different balance space than the intracellular metabolites), c_{in} (related to A_{feed}) is the input concentration of the controllable feed flux v_{feed}. Notice that, according to equation (1) here $\beta = (c_{in}, v_{feed}, V_{intra}, V_{extra})$. The term v_{upt} is the uptake flux as defined in Table III. The extracellular substrate A_{ex} is then taken up by a transport mechanism v_{upt} which exhibits product inhibition (via A). The intracellular metabolite A reacts to metabolite B by a reversible Michaelis-Menten kinetic function. The bimolecular reactions v_2 uses the substrates B and E to produce C. This reaction follows a Hill type kinetic function. The reversible reaction v_5 refills the metabolite pool E. Metabolite C is consumed by reaction v_3, producing D and F. The reaction is inhibited by high D concentrations. D can be degraded to E and F by reaction v_4, which is inhibited by C. The export of E is facilitated by reaction v_6, following Michaelis-Menten kinetics. Unlike [19], this study excludes v_7 and the metabolite F_{ex}, since F_{ex} has dynamics that are very similar to E_{ex}. Furthermore, exchange fluxes have not been considered, thus the study is limited to the net flux of v_1 and v_5. The kinetic equations used to simulate the network for the testcase are shown in Table III, whereas the parameters are given in Table IV. The experimental conditions studied in [19] are modified in the present work: rather than focusing on a single, highly concentrated pulse, a series of different input signals is studied and compared: these, as well as the experimental parameters used for the test case (accounting for the β term in (1)) are described in Table 3. This network also contains C-atom transformations by bimolecular and splitting reactions, as depicted in Fig. 1 (right). In particular, as discussed previously, the bimolecular reaction step v_2 generates nonlinearities in the isotopomer balances. For the current study it is assumed that all intracellular metabolite pools can be quantified, including all mass isotopomer fractions. Additionally the extracellular substrate concentration as well as the product E_{ex} can be measured.

2.5. Piecewise Affine Models

We are interested in providing an approximation of the system of ODE in (1)-(2) describing the dynamics of metabolite concentrations and (labeled) isotopomer fractions. This work employs a class of autonomous dynamical models, known as piecewise affine [43, 44], as follows:

$$\left\{ \begin{array}{l} \dot{c} = Nv(c,\alpha,\beta) \\ \dot{x} = D(c)^{-1} g(c,x,\alpha,\beta) \end{array} \right. \quad \text{is approximated as} \quad \left(\begin{array}{c} \dot{c} \\ \dot{x} \end{array} \right) = A_i \left(\begin{array}{c} c \\ x \end{array} \right) + b_i. \tag{4}$$

Here the state variable $z = (c,x)^T \in \mathbb{R}^n, n = \mathfrak{c} + \sum_{j=1}^{\mathfrak{c}} 2^{\iota(c_j)}$, thus $A_i \in \mathbb{R}^{n\times n}$ and $b_i \in \mathbb{R}^n$. For both models, the measurable output is given by the quantities $(c_i, c_{i+r}), i = 1,\ldots,\mathfrak{c}, r = 0,\ldots,\iota(c_i)$ representing measured unlabeled and labeled concentrations. Furthermore, the state variable $z \in \Omega_i, i = 1,\ldots,\mathfrak{p}$, $\Omega_i \subseteq \mathbb{R}^n, \Omega_i \cap \Omega_j = \emptyset, i \neq j, t \in \mathcal{T}$. In other words the domain of definition $\mathbb{R}^n$ is partitioned within $\mathfrak{p}$ non-overlapping regions Ω_i, within each of which the dynamics appear with the form $A_i z + b_i$, which is a linear-plus-offset (affine) function. It is assumed that the vector fields are Lipschitz continuous over $\mathbb{R}^n$, and in particular continuous over the boundaries of the regions Ω_i. For more details on PWA models, please refer to [25].

The parameters of the PWA approximation in (4) are related to the parameters α of the model in (1)-(2). The objective of an identification problem is, given a structure for the dynamics $(v(c,\alpha,\beta))$ and measured data provided by various experiments (each characterized by a parameter set β), to determine optimal parameters (α) for the dynamics. This is also the main goal of the present study: that of selecting optimal A_i, b_i, Ω_i for the PWA approximation, based on experimental data.

3. IDENTIFICATION OF DYNAMIC FLUX PROFILES

This section describes the approximation of time dependent concentrations and flux profiles with (time dependent) PWA models.

3.1. Time-dependent Flux Identification

Given a time series of measured labeled concentrations $c_i(t)y_{i,r}(t), t \in \mathcal{T}_m, i = 1,\ldots,\mathfrak{c}, r = 0,\ldots,\iota(c_i)$, we are interested in approximating these signals by parameterized functions $\hat{c}_i(t,\theta)\hat{y}_{i,r}(t,\theta)$ obtained from the time-dependent flux vector $\hat{v}(t,\theta)$ according to the dynamics in (1)-(2). Here $\hat{v}(t,\theta)$ is a $\mathfrak{v}$-dimensional vector of approximated flux functions and θ a vector of parameters to be defined shortly.

This study introduces a PWA expression for the quantity $\hat{v}(t,\theta)$. However, unlike in (4) where the (c,x)-state space is partitioned, notice that at this stage the partitioning is introduced over the time domain $\mathcal{T}$. More precisely, each of the $\mathfrak{v}$ approximated flux functions $\hat{v}_i(t,\theta_i)$ is defined over $\mathcal{T}$ as:

$$\hat{v}_i\,(t,\theta_i) = \left\{ \begin{array}{lll} \theta_i^1 \left[\begin{array}{c} t \\ 1 \end{array} \right] & \text{if} & t_0 \leq t < t_1, \\ \vdots & & \vdots \\ \theta_i^{\mathfrak{p}} \left[\begin{array}{c} t \\ 1 \end{array} \right] & \text{if} & t_{\mathfrak{p}-1} \leq t \leq t_{\mathfrak{p}}. \end{array} \right. \tag{5}$$

Here $i = 1,\ldots,\mathfrak{v}$ indicates the specific flux; $\mathfrak{p}$ is the total number of regions characterized by $t_0 = 0 < t_1 < \ldots < t_{\mathfrak{p}} = T$: there are $\mathfrak{p} - 1$ switching events that make up the set

$\mathcal{T}_s \doteq \{t_1, \ldots, t_{\mathfrak{p}-1}\}$; $\theta = [\theta_1, \ldots, \theta_{\mathfrak{v}}]^T$ is the vector of parameters that one is interested in for the optimization problem (it is related to α in (1)), where $\theta_i = [\theta_i^1, \ldots, \theta_i^{\mathfrak{p}}]$ and θ_i^j are pairs $\theta_i^j = [\theta_i^{j,1}\, \theta_i^{j,2}]$. Notice that a single switching sequence $\mathcal{T}_s$ is applied (in parallel) to all the $\mathfrak{v}$ fluxes: this is grounded on computational reasons and on simulation outcomes, but by no means technically necessary. Furthermore, let us remark the difference between the sets $\mathcal{T}_m$ (measured samples) and $\mathcal{T}_s$ (switching times), both of which are finite subsets of the continuous time horizon $\mathcal{T}$. Continuity assumptions on the PWA approximation are raised, which result in the following:

$$\lim_{t \uparrow t_j} \theta_i^j \begin{bmatrix} t \\ 1 \end{bmatrix} = \theta_i^{j+1} \begin{bmatrix} t_j \\ 1 \end{bmatrix} \quad \Rightarrow \quad \theta_i^{j,1} t_j + \theta_i^{j,2} = \theta_i^{j+1,1} t_j + \theta_i^{j+1,2}, \qquad (6)$$
$$j = 1, \ldots, \mathfrak{p}-1, \quad i = 1, \ldots, \mathfrak{v}.$$

Over the $\mathfrak{p}$ regions and for each of the $\mathfrak{v}$ fluxes, due to the continuity constraints a total of $\mathfrak{v}(2\mathfrak{p} - (\mathfrak{p}-1)) = \mathfrak{v}(\mathfrak{p}+1)$ free parameters making up θ is obtained.

Given a switching sequence $\mathcal{T}_s = \{t_1, \ldots, t_{\mathfrak{p}-1}\}$, let us introduce the following errors $\epsilon_{i,r}(k, \theta), k \in \mathcal{T}_m$, over the labeled concentrations

$$\epsilon_{i,r}(k, \theta) = c_i(k) y_{i,r}(k) - \hat{c}_i(k, \theta) \hat{y}_{i,r}(k, \theta), \quad i = 1, \ldots, \mathfrak{c}, \quad r = 0, \ldots, \iota(c_i),$$

and the following minimization problem

$$\theta^* = \arg\min_{\theta} \sum_{k \in \mathcal{T}_m} \epsilon(k, \theta)^T W \epsilon(k, \theta), \qquad (7)$$

given the constraints in (6) and where $\epsilon(k, \theta)$ is a vector composed by the elements $\epsilon_{i,r}(k, \theta)$. The quantities $\hat{y}_{i,r}(k, \theta)$ are samples taken over $\mathcal{T}_m$ from the observation vector $\hat{y}(t, \theta), t \in \mathcal{T}$, which is a linear combination of the vector x ($(x \in \mathbb{R}^{\sum_{j=1}^{\mathfrak{c}} 2^{\iota(c_j)}}$, ref. Sec. 2)) of isotopomer fractions and is derived from the nonlinear and high-dimensional dynamics $\frac{dx}{dt} = D(c)^{-1} g(c, x, \alpha, \beta)$. Similarly, the quantities $\hat{c}_i(k, \theta)$ are derived from $\hat{c}(t, \theta), t \in \mathcal{T}$, which is obtained as $\hat{c}(t, \theta) = \hat{c}(0, \theta) + \int_0^t N \hat{v}(s, \theta) ds$. Furthermore, $W \in \mathbb{R}^{\sum_{j=1}^{\mathfrak{c}} 2^{\iota(c_j)} \times \sum_{j=1}^{\mathfrak{c}} 2^{\iota(c_j)}}$ is a diagonal weighting matrix (made up of positive elements), which is used to bias the cost function. This weight can be used to enhance certain labeled metabolite concentrations over others, or can be chosen according to measurement error levels associated to the single concentrations (W can also be made dependent on the samples $k \in \mathcal{T}_m$). We also introduce constraints over the approximated labeled concentrations, which have to be necessarily non-negative: $\hat{c}_i(k, \theta) \hat{y}_{i,r}(k, \theta) \geq 0, \forall k \in \mathcal{T}_m$. The unlabeled case is a special case of the labeled study above: we introduce the minimization problem in (7), where the parameter-dependent function $\epsilon(k, \theta)$, defined over $\mathcal{T}_m$, is vector valued (of dimension $\mathfrak{c}$) and defines the error over the concentrations:

$$\epsilon_i(k, \theta) = \left(c_i(k) - \hat{c}_i(k, \theta)\right), \quad i = 1, \ldots, \mathfrak{c}.$$

In the unlabeled case, given a switching sequence $\mathcal{T}_s$, by explicit integration in time of (5) according to (1), it is possible to express the functions $\hat{c}(k, \theta)$ – and thus also $\epsilon(k, \theta)$ – as linear functions of the parameter set θ. Given the linear constraints on the fluxes and on the concentrations, the quadratic problem in (7) can be globally solved and its solution θ^* can be easily computed with standard optimization software. For the labeled case, this optimization is in general nonconvex over θ due to the nonlinear dynamics in (2), and can be performed locally via Taylor expansions. Being a nonlinear problem, local minima may exist. Hence, a

multistart initialization and a proper choice of the initial conditions (e.g. when prior knowledge on the parameters exists) is desirable. This study has initialized the parameters θ for the labeled experiments based on the optimal set obtained from the unlabeled study run with the unlabeled dynamics in (1) (ref. Sec. 5). This has allowed to obtain a numerically feasible solution for the isotopomer differential equation (2).

Given a particular $\mathfrak{p}$-dimensional partitioning of the interval $\mathcal{T}$, characterized by the set $\mathcal{T}_s = \{t_1, \ldots, t_{\mathfrak{p}-1}\}$, the solution of the optimization problem (7) yields an optimal set of parameters θ^*. In the following, three algorithms are described to come up with a sequence of switching times $\mathcal{T}_s$ that adapts to the measured data and to the quality of the approximation. The first two (described in Sections 3.1.1 and 3.1.2) compute the switching times sequentially and are based on error trends, whereas the third one (presented in Section 3.1.3) directly looks at the derivative of the measured concentrations with no error calculation. The algorithms are presented for the labeled case, the unlabeled version being a special instance.

3.1.1. Error Interpolation (sequential) The first procedure (Algorithm 1 in the Appendix) selects the $\mathfrak{p}-1$ switching instants sequentially and is based on an interpolation over time of the errors $\epsilon(k,\bar{\theta}), k \in \mathcal{T}_m$, given a parameter vector $\bar{\theta}$. For each of the i metabolites, $i = 1, \ldots, \mathfrak{c}$ and of the mass isotopomer fractions $r = 0, \ldots, \iota(c_i)$, the error $\epsilon_{i,r}(k,\bar{\theta})$ is summed over the measurement times set $\mathcal{T}_m$ to yield the weighting parameter $E_{i,r}, E_{i,r} \doteq \sum_{k\in\mathcal{T}_m} \epsilon_{i,r}(k,\bar{\theta})$. Thereafter, selecting the largest of the weights $(i^*, r^*) = \arg\max_{i=1,\ldots,\mathfrak{c};r=0,\ldots,\iota(c_i)} E_{i,r}$, the maximum of the error $\epsilon_{i^*,r^*}(k,\bar{\theta}), k \in \mathcal{T}_m$, is calculated over time (this happens at time $t^* \in \mathcal{T}_m$) for metabolite i^* and mass fraction r^*. Based on this maximum, the time point in $\mathcal{T}$ preceding t^* where the error intercepts the zero axis (name it $t^\star$) is found via linear interpolation as:

$$t^\star = \inf \Big\{ t \in \mathcal{T} : t = |\alpha t_m + (1-\alpha) t^*|, \qquad (8)$$
$$t_m = \max\{k \in \mathcal{T}_m, k < t^* : \epsilon_{i^*,r^*}(k,\bar{\theta}) \leq 0 \vee k = t_0\}, \alpha \in [0,1] \Big\}.$$

The steps above always yield a time point $t^\star$ which is such that $t^\star \geq t_0$. If the interpolated point t_k is distanced from other existing switching times more than a chosen tolerance δ, the intercept is selected as the new switching point, otherwise the calculation is repeated with the second largest weight element $E_{i,r}$. Algorithm 1 is easily shown to yield feasible outputs and to terminate in a finite number of steps.

3.1.2. Clustering (sequential) Similar to the algorithm detailed in Section 3.1.1, a second procedure is also based on the time-dependent errors for each metabolite and mass fraction. A set $\mathcal{Z}$ is defined, which is valid for all the pools concentrations and is made up of all the time points associated to an error signal being equal to zero (practically, within a proper tolerance δ_1). Each element in this set is given a weight that is proportional to the sum of all measured errors up to the next element in time in $\mathcal{Z}$. The `k-means` algorithm [45] then creates clusters over the elements of $\mathcal{Z}$. (The number of clusters depends on the discussed weights.) The mean values associated to each cluster are added to the set of switching times $\mathcal{T}_s$. Since the contribution from all the metabolites are included in creating the set $\mathcal{Z}$, the algorithm allows for a global selection of the time switches for $\mathcal{T}_s$. The procedure is detailed in Algorithm 2 in the Appendix, which can again be shown to yield feasible outcomes and to terminate within a finite number of steps.

3.1.3. Concentration Trends (batch) An alternative algorithm for selecting the time switches in $\mathcal{T}_s$ employs the trends in time of the labeled concentration levels. This is in contrast to Algorithms 1 and 2, which focused on the magnitude of the errors as a function of time. Large time derivatives in labeled concentration levels are often associated with significant changes in the related fluxes, for instance when a saturation occurs or a sudden burst in substrate level is experienced. Similarly, it is of interest to detect situations where the derivative of a labeled concentration level is persistently small, which is related to the steady-state of the related fluxes. Trends are found by numerically computing the forward time difference over the labeled metabolite concentration levels. Algorithm 3 in the Appendix details the procedure, which is a batch algorithm and thus does not depend on an iterated mechanism. On the other hand, the presence of noise on the concentrations potentially disrupts the approach, and the lack of a iterative procedure may lead to locally suboptimal outcomes.

4. RECONSTRUCTION OF KINETIC EQUATIONS VIA PWA APPROXIMATIONS

In this Section the kinetic equations are identified based on the time-dependent functions obtained in Section 3. With reference to the dynamics in equation (1) and with the additional information provided by the identified PWA dynamics of $\hat{v}(t,\theta^*)$ and of $\hat{c}(t,\theta^*), t \in \mathcal{T}$, the problem of reconstructing the concentration-dependent enzyme kinetic equation $v(c,\alpha,\beta)$ as $\hat{v}(\hat{c},\vartheta,\Omega)$ is investigated. The parameters ϑ,Ω will be specified shortly.

The embedding is performed as visualized for an arbitrary flux dependent on two concentrations in Figure 2. First the profiles of the approximated concentrations are combined within the concentration space by "eliminating" their time dependence. An additional dimension is added to accommodate for the approximated flux profile: this returns a flux function over the concentration space. This procedure generates data for the identification of concentration-dependent kinetic equations describing the flux functions. Note that the approach uses, along with the approximated flux profiles $\hat{v}(t,\theta^*)$, also the approximated concentrations $\hat{c}(t,\theta^*), t \in \mathcal{T}$, rather than the original concentration measurements $c(t), t \in \mathcal{T}_m$: this enables using a larger set of data points than exclusively those in $\mathcal{T}_m$.

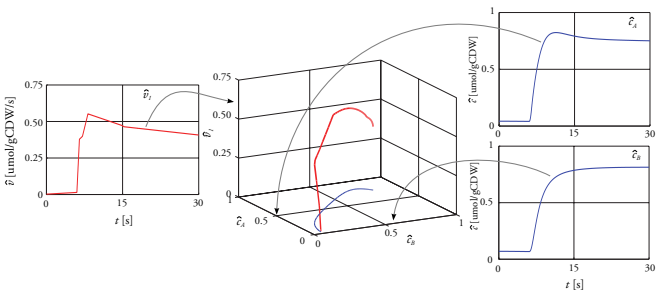

Figure 2. From the data generated by the two approximated concentrations a profile is created over the concentration space. Assuming a known interaction stoichiometry (namely, what metabolites influence what flux), the approximated flux profile is expressed over the concentration space.

Classical identification techniques assume a known equation layout such that nonlinear regression for parameter estimation can be used [34, 46]. This study instead aims at reconstructing kinetic equations without prior knowledge on the actual equation layout – only the interaction stoichiometry is taken to be known. More specifically, the goal is to approximate

the nonlinear equation $v_j(c_i, \alpha, \beta)$ by a PWA function

$$\hat{v}_j\left(\hat{c}_i(t), \vartheta_j, \Omega_j\right) = \begin{cases} \vartheta_j^1 \begin{bmatrix} \hat{c}_i(t) \\ 1 \end{bmatrix} & \text{if} \quad \hat{c}_i(t) \in \Omega_j^1, \\ \vdots & \vdots \\ \vartheta_j^{\mathfrak{p}} \begin{bmatrix} \hat{c}_i(t) \\ 1 \end{bmatrix} & \text{if} \quad \hat{c}_i(t) \in \Omega_j^{\mathfrak{p}}, \end{cases} \tag{9}$$

where j denotes a flux, $j = 1, \cdots, \mathfrak{v}$, and $i \in \gamma(j)$, where $\gamma : \{1, \ldots, f\} \to 2^{\{1,\ldots,\mathfrak{c}\}}$ is a set-valued map that associates to each flux a set of concentrations according to the known stoichiometry of the system. Furthermore, $\hat{c}_i(t) \in \mathbb{R}^{d(j)}, d(j) = \texttt{card}(\gamma(j)) \leq \mathfrak{c}$, represent the concentration samples, which are drawn from $\mathcal{T}$. The set of parameters referring to flux j is $\vartheta_j = \left[\vartheta_j^1, \ldots, \vartheta_j^{\mathfrak{p}}\right]$, where $\vartheta_j^i = \left[\vartheta_j^{i,1}, \ldots, \vartheta_j^{i,d(j)+1}\right]$, and depends on the selected domains $\Omega_j^i \subseteq \Omega_j \subset \mathbb{R}^{d(j)}$, where $\Omega_j^i \cap \Omega_j^l = \emptyset, \forall i \neq l$, $l = 1, \cdots, \mathfrak{p}$, and $\cup_{i=1}^{\mathfrak{p}} \Omega_j^i = \Omega_j$. Usually, Ω_j is given by the cross product of intervals over concentrations, $\Omega_j = [0, c_1] \times \ldots \times [0, c_{d(j)}]$. It is assumed that the PWA approximation is continuous over the boundaries of the partitions of Ω_j. Notice the similarity between (9) and (5). However for $\hat{v}_j\left(\hat{c}_i(t), \vartheta_j, \Omega_j\right)$ we shall optimize over both the parameters and the partitions, whereas for $\hat{v}_i\left(t, \theta_i\right)$ we searched for an optimal $\mathcal{T}_s$ defining the switching sequence and, given any $\mathcal{T}_s$, we optimized just over the parameters θ_i. In the present instance, the optimal parameter set ϑ_j and domains in Ω_j are sought so that they optimally describe the function $v_j(c_i, \alpha, \beta)$ by approximating it with equation $\hat{v}_j\left(\hat{c}_i, \vartheta_j, \Omega_j\right)$ in (9). Let us denote the global set of parameters as $\vartheta = [\vartheta_1, \cdots, \vartheta_f]^T$ and $\Omega = [\Omega_1, \cdots, \Omega_f]^T$.

A number of methods have been proposed to solve identification problems related to PWA functions [47, 48]. This works leverages either a *clustering approach* [35], or a *bounded error method* [36], both of which are supported by existing software toolboxes, respectively HIT [49] and PWAid [50]. We have integrated the two software tools, adapting a few algorithms within them. The Appendix contains a description of the methods in [35, 36] and of the developed software, and elaborates on the fundamental issue of data excitation for the model identification procedure. An application of the two identification approaches is developed in Section 5.

5. APPLICATION TO A METABOLIC CASE STUDY

The techniques in Sections 3 and 4 are applied to a metabolic network case study.

5.1. Dynamic Inputs for Benchmark Case Study

The metabolic network used for the in silico test case is depicted in Figure 1 and first introduced in Section 2.4. The kinetic equations used to simulate the metabolic network are taken from [19] and recapitulated in the Appendix — however, these functions are used only to generate data and for comparison with the outcomes of the methods.

For the test case, three realistic input profiles for the feed flux are used to simulate different dynamic experiments. Let us describe the operational parameters β, as in Section 2.4. The tunable parameters are the volume ratio V_R between the extra- and intracellular concentrations (V_{intra}, V_{extra}) within the reactor, and the influx of substrate v_{feed} with its concentration c_{in}. Both v_{feed} and c_{in} are time varying, so that a dynamic experiment is simulated by varying the labeling of the input: each experiment commences in steady state until the start of the

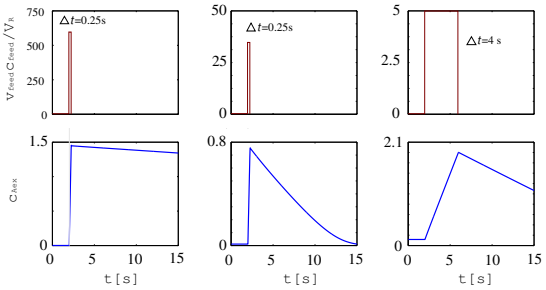

Figure 3. Three different input profiles are used to generate experimental data via simulations. The volume ratio $V_R(1/100, 1/10, 1/10)$ represents the ratio between the intracellular and extracellular volume (in practice, the ratio between cell and reactor volume). The influx $v_{feed}[L/s]$ is the (controllable) feed of extracellular substrate into the reactor. The influx the feed concentration $c_{in}[mmol]$ is also controllable. The organism is kept unlabeled and at steady state until $\tau_{f1} = 2[s]$, after which a pulse of labeled substrate is added until $\tau_{f2} = \tau_{f1} + \Delta t$, when the feed is switched off.

feed input at time $t = \tau_{f1}$. Next, a labeled pulse or gradual increase of the extracellular concentration is created for $\tau_{f1} \leq t < \tau_{f2}$, after which the influx is set to zero. A total of three different input profiles are created, as recapitulated in Figure 3. Based on these inputs, data sets are generated as measurements of concentrations and of mass isotopomer fractions. The study considers rapid measurement sampling with frequency of 1 Hz, and an artificial noise corresponding to 2% of the signal magnitude is added to the dynamics. The simulations will result in concentration data $c(t) \in \mathbb{R}^{(\mathfrak{m}+1)\times\mathfrak{c}}$, mass isotopomer fractions $y(t) \in \mathbb{R}^{(\mathfrak{m}+1)\times\sum_{j=1}^{\mathfrak{c}}(\iota(c_j)+1)}$, over a set of discrete sample times $t \in \mathcal{T}_m = \{t_0^m, \cdots, t_{\mathfrak{m}}^m\}$. Here $\mathfrak{m}+1$ is the number of time samples, $\mathfrak{c}$ is the number of metabolite concentrations, and $\iota(c_j)+1$ is the number of mass isotopomer fractions for the labeled concentration c_j, which depends on the number of carbon atoms of the corresponding metabolite.

For the test case, the washout term is omitted (namely, we assume that $c_{A_{ex}} = 0$). Furthermore, it is assumed that all intracellular metabolite pools can be quantified (including all mass isotopomer fractions), along with the extracellular substrate concentration and the product E_{ex}. Notice that the case study excludes v_7 and the metabolite F_{ex}, since F_{ex} has dynamics that are very similar to E_{ex}. Exchange fluxes have not been considered, thus the study is limited to the net flux of v_1 and v_5. Altogether, this results in 8 kinetic functions for the unlabeled part, and 8 metabolites with a total of 26 mass isotopomers. The number of parameters for the PWA approximations in time is in the order of 50.

5.2. Reconstruction of dynamic flux profiles in time

Before carrying out the time-dependent reconstruction, a search for the global minimum over both parameter set θ and switching sequence $\mathcal{T}_s$ is performed, to set a benchmark for the ensuing study. For the unlabeled case, the optimization problem is used as an objective function for a global genetic algorithm, which includes the switching sequence $\mathcal{T}_s$ as a variable. In order to avoid suboptimal results, the genetic algorithm is executed with random initial conditions 50 times for each of the three input sets, and for $\mathfrak{p} = 3, 4, 5$ switches in $\mathcal{T}_s$. As a side result, this global optimization has given useful recommendations on additional information to be used for the later reconstruction, such as the placement in time of the first switch with reference to parameters τ_{f1}, τ_{f2}, and the minimal distance between adjacent switches (parameters δ in Algorithm 1, and δ_2 in Algorithms 2 and 3). The complete cohort of experiments for the

genetic algorithm has run in about a day with a MATLAB `ga` procedure, over a cluster of four desktops with Intel processors, 2.5GHz and 2GB RAM. The genetic algorithm turns out to be computationally too demanding for the labeled case and is thus left out for this latter setup.

5.2.1. Switch allocation methods: unlabeled case

As anticipated, in all the experiments the following additional information, which is gathered from the runs with the genetic algorithm as well as from the specific experimental setup, is embedded:

- since the dynamic experiments are started in the (unlabeled) steady-state, for any metabolite i the value of the constants $\hat{c}_i(0,\theta) = \sum_j N(i,j)\theta_j^{1,2}$ will be determined based on the first value of the corresponding metabolite concentration
- a 0^{th}-order (flat) profile is enforced for the first domain of the approximated flux profile, since all data sets start from steady state ($\theta_i^{1,1} = 0, i = 1, \ldots, \mathfrak{v}$)
- the feed start is associated by default to a switch
- no switches are allowed to be allocated in the very last second of the time horizon
- a threshold of 0.5 seconds is used to separate adjacent switches (with an exception for the switches placed close to the feed start)

The three different switch allocation methods are compared and benchmarked against the runs of the global genetic algorithm. The algorithms can select either 3, 4, or 5 switches ($\mathfrak{p}$). The results are displayed in Table I for the case of $\mathfrak{p} = 5$. The tables display the errors over both concentrations and fluxes. (Note again that the comparison between actual and approximated fluxes is possible for the case under study since the structure of the kinetic equations is known.)

Allocation of 5 switches in the unlabeled case

	Error on concentrations c					Error on fluxes v				
	GA (c)	GA (v)	S.1	S.2	B.1	GA (c)	*GA (v)*	S.1	S.2	B.1
Set 1	*4.48*	5.61	4.78	4.58	4.57	12.86	*1.06*	6.95	6.89	5.47
Set 2	*0.99*	2.75	2.36	25.94	1.86	21.93	*0.94*	6.72	101.64	2.80
Set 3	*1.84*	3.58	2.28	2.32	2.59	4.15	*0.06*	2.62	2.42	0.94

Table I. Errors between the approximated and measured concentrations (left), and between the approximated and real fluxes (right) for PWA approximations with 5 switches on unlabeled data. GA (c) is the minimum of 50 runs of a genetic algorithm that minimizes the difference between measured and approximated concentration. Similarly, GA (v) minimizes the difference between known and approximated fluxes. The left part of the table compares the errors over the *concentrations*, for the different methods, whereas the right table displays the errors of the difference between known and approximated fluxes (the corresponding italicized columns are the benchmark for the theoretical minimum). S.1 is the error interpolation procedure, S.2 the clustering method (S.1 and S.2 are sequential), and B.1 the batch method based on concentration trends. The green numbers denote the best method for each of the three datasets.

Comparing the outcomes of three switch allocation methods, it can be definitely concluded that the batch method, which is based on the computation of the numerical derivative of the metabolites concentrations, it the one that leads to the best performance. Furthermore, being a one-shot technique (rather than sequential in nature), it also beats the other two methods computationally: the computational time for the allocation of 5 switches, for each of the three experiments, are respectively 19.90, 15.88 and 4.48 seconds. The results are obtained on an

Intel c2d T9300 processor, with 2.5GHz and 2GB RAM. The output of the first sequential technique has, in a few instances, also shown some issues related to overfitting, particularly in the case of bidirectional fluxes with fast dynamics: this is a problem that is due to the network structure, rather than to the mathematical approach. A solution can be found by fixing the exchange flux at a high level and estimating only the net fluxes. In general the performance of the batch technique, which depends on a numerical computation of the derivative, may be disrupted in case the measured data comes with high noise levels.

5.2.2. Switch allocation methods: labeled case

The labeled case is studied similarly to the unlabeled case of Section 5.2.1. The experimental setup and embedded additional information is also analogous. Recall that the genetic algorithm is not feasible for the dimensions and complexity of the labeled network. The labeled optimization problem requires a feasible initial parameter set, since in order to obtain a numerically meaningful solution for the isotopomer differential equation the pool concentrations have to be strictly positive. The parameters for the labeled experiments are thus initialized based on the optimal set obtained from a run of the unlabeled study, which is based on the optimization problem (7) defined over unlabeled concentrations and run with the unlabeled dynamics. For the sequential methods this entails to solve an unlabeled problem at the first iteration step, after which the labeled optimization problem is executed for each remaining iteration. The batch method requires no iterations, thus the unlabeled problem is run first, then the labeled one is executed. As in the unlabeled case, the initial conditions for the variables c, x are taken from measurements (concentrations) and from the natural labeling of the isotopomer states.

Due to space limitations, only the scenario with five switches is presented in Table II. Notice that since the values in this table represent the accrued error of the *labeled* concentrations in the value function of the optimization problem (7), which includes also the contribution from the isotopomer mass fractions, they cannot be directly compared to the values presented in Table I.

A few observations can be made. The error on the labeled concentrations is reduced by using the labeled optimization problem (cfr. Table II, left vs right column): thus the solution of the labeled problem yields results that are more accurate than the unlabeled one. The batch method and the first sequential method perform similarly (cfr. Table II, right column). It is interesting to note that in two of the three experiments the labeled results improve the unlabeled outcomes — this again motivates resorting to the labeled scenario. As expected, the computational time required to solve the labeled problem has increased. Increasing the size of the network or the number of carbon atoms of the substrate (which is also related to an increase of the network size) directly impacts the computational times. The computational times required for the three experiments (initialization runs are excluded) are on average respectively $35.3, 41.7$, and 7.9 minutes: the batch method is still the fastest. Results are obtained on an Intel c2d T9300 processor, with 2.5GHz and 2GB RAM. The procedure for the labeled case is computationally much heavier than that for the unlabeled scenario.

5.2.3. Reconstruction of dynamic profiles

Since the batch method appears on overall to yield the best results, Figures 4 and 5 display its outcomes for the third experimental scenario (as per Figure 3) over a labeled network. It can be observed that the flux and concentration approximations are quite accurate. Outcomes with similar performance have been obtained for the first two input sets.

Allocation of 5 switches in the labeled case

	Errors on cy unlabeled optimization			Errors on cy labeled optimization		
	S.1	S.2	B.1	S.1	S.2	B.1
Set 1	6.46	4.74	1.95	0.77	4.74	1.94
Set 2	5.62	6.06	6.22	5.62	6.06	6.22
Set 3	0.07	0.09	0.07	0.05	0.05	0.04

Table II. Errors between the approximated and measured labeled concentrations. The left column displays the results of the initial unlabeled optimization, while the right figures refer to the labeled optimization. For the labeled case there is no available benchmark from the genetic algorithm. The data is ordered similarly to Table I.

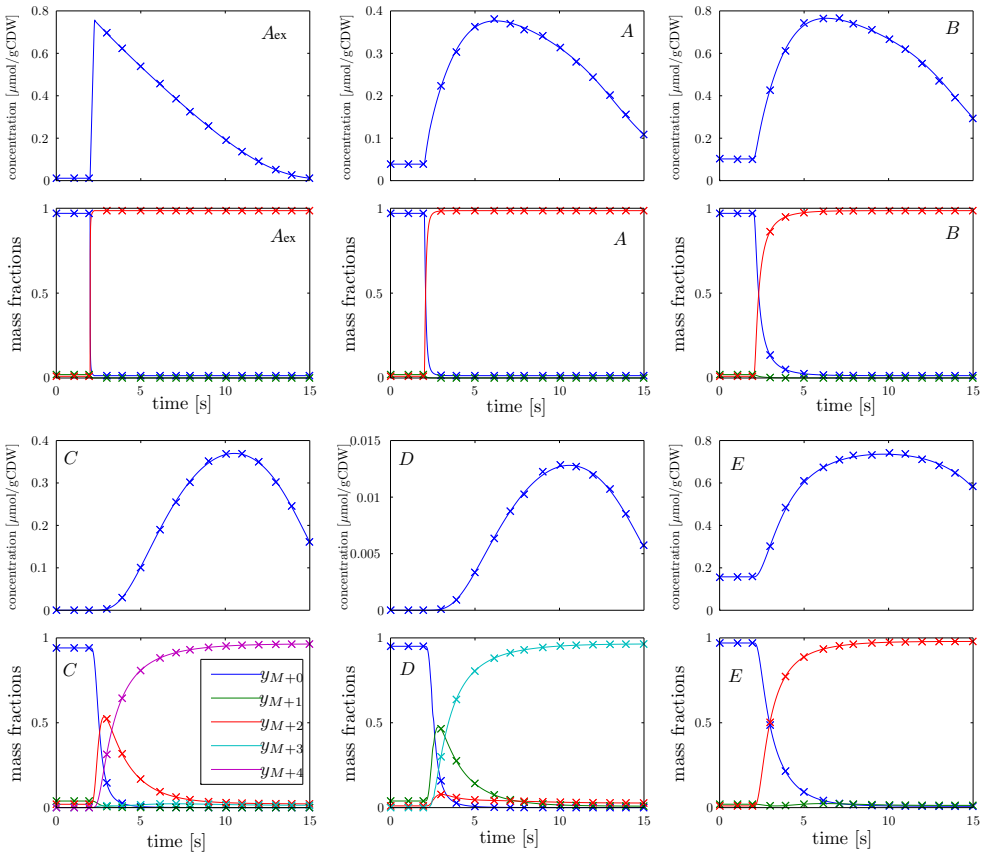

Figure 4. Reconstruction of labeled concentration profiles using the batch method for the switch allocation. The figure shows the measurements (crosses) and the approximations (lines), for metabolites A_{ex} and A to E. The graphs display both the mass isotopomer fractions (y_{M+r} on the bottom plots, for a generic metabolite M and where $r = 0, \ldots, 4$ denotes the weight difference; the plots are in absolute units) and metabolite concentrations (top plots, with units μmol/gCDW).

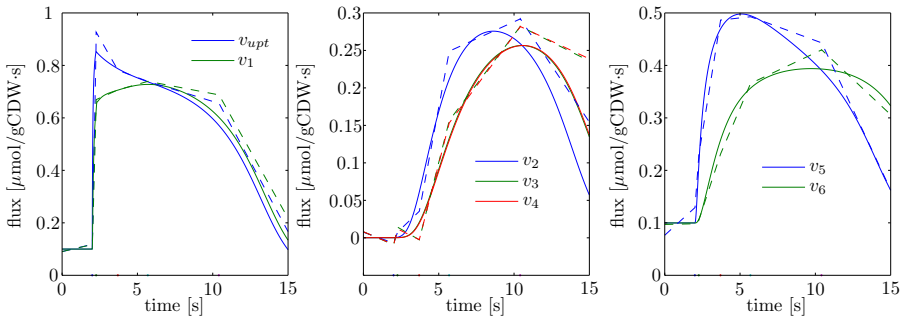

Figure 5. Reconstruction of flux profiles using the batch method for the switch allocation. This figure displays the actual flux profiles (continuous lines) and the PWA approximated profiles (dashed).

5.3. PWA Reconstruction of enzyme kinetic equations

The identified flux profiles in time, along with being of interest to the biologist since they shed light over the dynamic exchange of material among different labeled metabolites, represent also an integral part of the reconstruction of the enzyme kinetic equations as functions of the concentration levels.

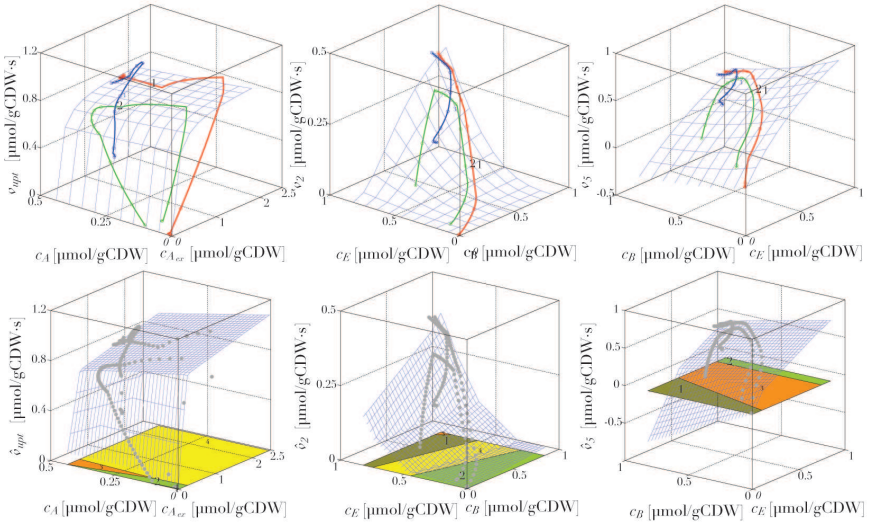

Figure 6. Top row – Reconstructed flux profiles in time (colored lines, one for each experiment) are embedded in the (approximated) concentration space. The shown fluxes – ordered per column: $\hat{v}_{upt}$, $\hat{v}_2$, and $\hat{v}_5$ – refer to the metabolic network of Figure 1. The overlaid grid displays the corresponding actual nonlinear enzyme kinetic equations (respectively v_{upt}, v_2, and v_5). Bottom row – The reconstructed PWA equations of the corresponding enzyme kinetic equations.

Each approximated flux profile is embedded in the corresponding concentration space. Recall that this embedding is performed over the approximated signals instead of the measured ones, since the former offer a larger amount of data to select from. Figure 6 (top row) displays the

set of three embedded flux profiles. For these fluxes the dynamics appear to be nicely excited, however this is not the case for all reconstructed fluxes: data may aggregate along lower-dimensional spaces. In general, exciting metabolite pools (particularly intracellular ones) that are related to these fluxes is hard. Thus, while it is in general very hard to estimate all the kinetic equations, the outcome may yield useful insight on the primary regulation mechanism for specific fluxes for which the reconstruction is not feasible. Notice that it is possible to generate additional information and embed it as newer data: for instance, this can be done if it is known that a kinetic equation is equal to zero or if it is known to saturate at a particular level corresponding to respectively low and high concentration levels of a certain metabolite.

We have reconstructed the kinetic equations in Figure 6 using the techniques in [49] and [50], which are discussed in the Appendix. The procedure has been repeated 50 times per method. For the HIT toolbox, the number of domains is varied between three and five. The relative error bound δ used in PWAid is varied within $\delta \in \{1/15, 1/25, 1/35\}$: its outcomes with three domains are used for a comparison with HIT. In HIT, the expected number of domains is a parameter chosen by the user. For PWAid, the error bound δ needs to be tuned to obtain a similar number of domains. All identifications runs result in outcomes with two to six domains. Since the computational demand is relatively low, the accuracy can be increased by considering models with higher number of domains. However, the enforcement of continuity may become heavy when a large number of modes is considered.

Of the two toolboxes, PWAid yields the best outcomes with regards to the minimal error (although the difference with HIT is marginal), however the average and standard deviation of the error in HIT is in general smaller than that in PWAid. Computationally, HIT seems to outperform PWAid. The possibility to specify the number of domains as an initial parameter is a valuable feature of HIT. The reconstructed PWA kinetic equations obtained by HIT are shown in Figure 6 (bottom row). The identified kinetic equations are quite accurate when compared to the original nonlinear equations used in the simulation: this especially holds for the regions in the state space where the embedded data is present.

6. CONCLUSIONS AND FUTURE WORK

This work has shown an application of the PWA framework in system biology: dynamic fluxes and kinetic functions have been identified from ^{13}C labeling experiments. The use of information from dynamic ^{13}C data is an essential extension of the dynamic flux estimation in [37], employed to identify fluxes at branch points, as well as bidirectional (fast-equilibrium) reactions. While adding to the information content of observed data, the use of ^{13}C labeling significantly increases the amount of equations and introduces non-linearity in the system dynamics: the computational complexity thus becomes critical for the proposed optimization procedure.

With regards to the reconstruction in time of flux profiles, our contribution has put forward three algorithms for their PWA approximation. These have been ranked over an informative test metabolic network. For the ranking, different experimental setups have been chosen (high/low pulses with fast/slow growth), and a benchmark PWA approximation has been calculated using a global genetic algorithm. It has been observed that experiments with a high dynamic range (first two setups) cannot be approximated as accurately as experiments with slower dynamics (third experiment). Furthermore, the dynamics have an essential influence on the minimal number of domains: while for the third experimental set four switches are sufficient, at least five are needed for the first two experiments. Quite surprisingly, for the

domain selection a batch approach has performed better than two sequential strategies. The sequential algorithms seem to be outperformed especially for experiments that result in highly dynamic flux profiles (first two sets). However, the performance of the batch technique may decrease for experimental setups affected by high levels of noise.

For the second step (identification of enzyme kinetic equations), two techniques in the literature with related software implementation have been tailored and integrated. Within the current implementation, it is possible to perform PWA reconstructions of continuous models (unlike the approximations proposed in [38]). This enables efficient comparison of different kinetic hypotheses and thus promises to improve the biological knowledge of *in vivo* enzyme kinetics.

Looking forward, the performance of the integrated procedure for flux profile reconstruction has to be further optimized and parallelized in order to be applied to biologically relevant, genome-scale networks with labeling enrichments.

APPENDIX

Time-dependent Flux Identification

We report the details of the three procedures for the reconstruction of dynamic flux profiles in time: Algorithm 1 (page 18), Algorithm 2 (page 19), and Algorithm 3 (page 19).

Algorithm 1 Error Interpolation

Require: maximum number of regions $\mathfrak{p}$, parameter δ

initialize set of time points $\mathcal{T}_s := \emptyset$, counter $l := 1$, and index set $C := \{(i,r) : i = 1,2,\dots,\mathfrak{c}; r = 0,1,\dots,\iota(c_i)\}$
while $l < \mathfrak{p} \wedge C \neq \emptyset$ **do**
  solve problem (7) and find optimal θ^*
  compute $(i^*, r^*) := \arg\max_{(i,r)\in C} E_{i,r}$, and $t^* := \max_{k\in\mathcal{T}_m} \epsilon_{i^*,r^*}(k,\theta^*)$, where $E_{i,r} := \sum_{k\in\mathcal{T}_m} \epsilon_{i,r}(k,\theta^*)$
  compute interpolation t_l according to (8)
  if $\min_{t\in\mathcal{T}_s} |t_l - t| > \delta$ **then**
    set $\mathcal{T}_s := \mathcal{T}_s \cup \{t_l\}$, $C := \{(i,r) : i = 1,2,\dots,\mathfrak{c}; r = 0,1,\dots,\iota(c_i)\}$, $l := l + 1$
  else
    $C := C \setminus \{(i^*, r^*)\}$
  end if
end while
return $\mathcal{T}_s$

PWA Identification Techniques

A number of methods have been proposed to solve identification problems related to PWA functions [47,48]. Among them, a *clustering approach* [35] employs prescribed model structures and allows identification of continuous functions, but it appears to get less accurate when the model order is unknown. A *bounded error method* [36] uses a desired accuracy and requires no prior knowledge on the model structure, but appears to be computationally more demanding. Both methods are supported by existing software toolboxes: HIT [49] and PWAid [50], respectively. In this work, we have integrated the two software tools and adapted a few procedures. Technically, both toolboxes require the MPT [39] — modifications within

Algorithm 2 Clustering

Require: maximum number of regions $\mathfrak{p}$, parameters δ_1, δ_2

initialize set of time points $\mathcal{T}_s := \emptyset$, counter $l := 1$
while $l < \mathfrak{p}$ **do**
  solve problem (7) and find optimal θ^*
  construct set $\mathcal{Z} := \{(i, r, z) : |\epsilon_{i,r}(z, \theta^*)| < \delta_1, i = 1, \ldots, \mathfrak{c}, r = 0, 1, \ldots, \iota(c_i), z \in \mathcal{T}_m\}$. $\mathcal{Z}$ has cardinality $\mathfrak{z}, \mathcal{Z} = \{(\cdot, \cdot, z_1), (\cdot, \cdot, z_2), \ldots, (\cdot, \cdot, z_\mathfrak{z})\}$
  define $E_i := \sum_{z_i \le k \le z_{i+1}, k \in \mathcal{T}_m} \epsilon_{j,r}(k, \theta^*)$, where $(j, r, z_i) \in \mathcal{Z}, j = 1, \ldots, \mathfrak{c}, r = 0, 1, \ldots, \iota(c_j), i = 1, \ldots, \mathfrak{z} - 1$, whereas $E_\mathfrak{z} := \sum_{z_\mathfrak{z} \le k \le t_n, k \in \mathcal{T}_m} \epsilon_{j,r}(k, \theta^*)$
  use `k-means` algorithm to group zeros $(\cdot, \cdot, z_i) \in \mathcal{Z}$ – weighted according to E_i – within n clusters, $\{z_i^1\}, \ldots, \{z_i^n\}$, each of which with mean $\mu^1, \ldots, \mu^n$
  $\mu^* := \arg\max_{i=1,\ldots,n} \sum_{j: z_j \in \{z_j^i\}} E_j$
  if $\min_{t \in \mathcal{T}_s} |\mu^* - t| > \delta_2$ **then**
    define set of time points $\mathcal{T}_s := \mathcal{T}_s \cup \{\mu^*\}, l := l + 1$
  else
    $l := \mathfrak{p}$
  end if
end while
return $\mathcal{T}_s$

Algorithm 3 Concentration Trends

Require: maximum number of regions $\mathfrak{p}$, parameters δ_1, δ_2

initialize set of time points $\mathcal{T}_s := \emptyset$
based on dynamics of $c_i(t) y_{i,r}(t), t \in \mathcal{T}_m, i = 1, \ldots, \mathfrak{c}, r = 0, 1, \ldots, \iota(c_i)$, compute finite set $\mathcal{Z} \in \mathcal{T}$ made up of local maxima of the numerical derivative, and start- or end-points for steady-state (based on zero crossing of numerical derivative according to tolerance δ_1)
use `k-means` algorithm to cluster points $z_{i,r} \in \mathcal{Z}$ within $\mathfrak{p}$ clusters, $\{z_{i,r}^1\}, \ldots, \{z_{i,r}^\mathfrak{p}\}$, each of which with mean $\mu^1, \ldots, \mu^\mathfrak{p}$; associate weight E_j to point μ^j as in Algorithm 2; sort values μ^j according to weight E_j so that $\bar{\mu}^1$ is the largest
for i=1,..., $\mathfrak{p}$ **do**
  if $\min_{t \in \mathcal{T}_s} |\bar{\mu}^i - t| > \delta_2$ **then**
    define set of time points $\mathcal{T}_s := \mathcal{T}_s \cup \{\bar{\mu}^i\}$
  else
    define set of time points $\mathcal{T}_s := \mathcal{T}_s$
  end if
end for
return $\mathcal{T}_s$

this toolbox have been performed in order to increase the robustness of the LP solvers.

The underlying assumption for a successful identification procedure is the "excitation" of the model dynamics: qualitatively, all states of the model ought to be excited in such a way that the full range of dynamics is displayed in the output data [51]. In the case of metabolic networks this entails the presence of enough data over the regions of the concentration space where kinetic equations are to be reconstructed. This requirement may be infeasible for a number of biological systems: for instance, the intracellular metabolite pools can only be excited up to certain levels. Furthermore, since the concentration and labeling data used for the identification is generated by dynamic experiments that always start in steady state, a single experiment will typically span a limited region of the space. In addition, while some fluxes are stoichiometrically dependent on several concentrations, in practice they may be mostly influenced by a single

one. While it is in general impossible to estimate a kinetic equation over all concentration ranges, a partial outcome may still yield useful insight on the primary regulation mechanism for the specific flux.

Kinetic equations

We report the structure (Table III) and the parameters (Table IV) of the kinetic equations, adapted from [19], for the network displayed in Figure 1.

Kinetic equations in the metabolic network of the case study

flux	mechanism	inhibitor	kinetic equation
v_{upt}	Michaelis-Menten, 1 inhibitor	A	$\frac{v_{max}c_{A_{ex}}}{\left(K_{mA}+c_{A_{ex}}\right)\left(1+\frac{c_A}{K_I}\right)}$
v_1	Reversible Michaelis-Menten		$\frac{v_{max}\left(c_A-\frac{c_B}{K_{eq}}\right)}{K_{mA}\left(1+\frac{c_B}{K_{mP}}\right)+c_A}$
v_2	2 Substrate Hill-Kinetic		$\frac{v_{max}c_B^{hA}c_E^{hB}}{\left(K_{mA}+c_B^{hA}\right)\left(K_{mB}+c_E^{hB}\right)}$
v_3	Michaelis-Menten, 1 competitive inhibitor	D	$\frac{v_{max}c_C}{K_{mA}\left(1+\frac{c_D}{K_I}+c_C\right)}$
v_4	Michaelis-Menten, 1 competitive inhibitor	C	$\frac{v_{max}c_D}{K_{mA}\left(1+\frac{c_C}{K_I}+c_D\right)}$
v_5	Reversible Michaelis-Menten		$\frac{v_{max}\left(c_B-\frac{c_E}{K_{eq}}\right)}{K_{mA}\left(1+\frac{c_E}{K_{mP}}\right)+c_B}$
v_6	Michaelis-Menten		$\frac{v_{max}c_E}{K_{mA}+c_E}$

Table III. Kinetic equations for the metabolic network of Fig. 1 (the parameters are in Table IV).

REFERENCES

1. Wohlgemuth R. The locks and keys to industrial biotechnology. *Nature Biotechnology* Apr 2009; **25**(4):204–213.
2. Hermann B, Blok K, Patel M. Producing bio-based bulk chemicals using industrial biotechnology saves energy and combats climate change. *Environmental Science & Technology* 2007; **41**:7915–7921.

Parameter values used to simulate the metabolic network of the case study

Reaction	Parameter	Value	Reaction	Parameter	Value	Reaction	Parameter	Value
v_{upt}	v_{max}	1	v_2	v_{max}	2.5	v_4	v_{max}	3
	K_I	3		K_{mA}	0.25		K_I	1
	K_{mA}	0.1		hA	2		K_{mA}	0.1
				K_{mB}	2			
				hB	3			
v_1	v_{max}	3	v_3	v_{max}	2	v_5	v_{max}	2
	K_{eq}	3		K_I	0.05		K_{eq}	4
	K_{mA}	0.1		K_{mA}	2		K_{mA}	1
	K_{mP}	3					K_{mP}	1
						v_6	v_{max}	2
							K_{mA}	3

Table IV. Parameters for the kinetic equations in Table III of the metabolic network of Fig. 1.

3. Hatti-Kaul R, Törnvall U, Gustafsson L, Börjesson P. Industrial biotechnology for the production of bio-based chemicals: a cradle-to-grave perspective. *Trends in Biotechnology* Mar 2007; **25**(3):119–124.
4. Hermann B, Patel M. Today's and tomorrow's bio-based bulk chemicals from white biotechnology: a techno-economic analysis. *Applied Biochemistry and Biotechnology* Mar 2007; **136**(3):361–388.
5. Nakamura C, Whited G. Metabolic engineering for the microbial production of 1,3-Propanediol. *Current Opinion in Biotechnology* Oct 2003; **14**(5):454–459.
6. Whited G, Feher F, Benko D, Cervin M, Chotani G, McAuliffe J, LaDuca R, Ben-Shoshan E, Karl J. Development of a gas-phase bioprocess for isoprene-monomer production using metabolic pathway engineering. *Industrial Biotechnology* 2010; **6**(3):152–163.
7. Wittmann C, Kiefer P, Zelder O. Metabolic fluxes in *Corynebacterium glutamicum* during lysine production with sucrose as carbon source. *Applied and Environmental Microbiology* 2004; **70**:7277–7287.
8. Park J, Lee S, Kim T, Kim H. Application of systems biology for bioprocess development. *Trends in Biotechnology* Aug 2008; **26**(8):404–412.
9. Kitano H. Systems biology: a brief overview. *Science* Mar 2002; **295**(5560):1662–1664.
10. Rizzi M, Baltes M, Theobald U, Reuss M. In vivo analysis of metabolic dynamics in *Saccharomyces cerevisiae*: II. mathematical model. *Biotechnology and Bioengineering* Aug 1997; **55**(4):592–608.
11. Theobald U, Mailinger W, Baltes M, Rizzi M, Reuss M. In vivo analysis of metabolic dynamics in *Saccharomyces cerevisiae*: I. experimental observations. *Biotechnology and Bioengineering* Jul 1997; **55**(2):305–316.
12. Magnus J, Hollwedel D, Oldiges M, Takors R. Monitoring and modeling of the reaction dynamics in the valine/leucine synthesis pathway in *Corynebacterium glutamicum*. *Biotechnology Progress* 2006; **22**(4):1071–1083.
13. Oldiges M, Kunze M, Degenring D, Sprenger GA, Takors R. Stimulation, monitoring, and analysis of pathway dynamics by metabolic profiling in the aromatic amino acid pathway. *Biotechnology Progress* 2004; **20**(6):1623–1633.
14. Wahl S, Haunschild M, Oldiges M, Wiechert W. Unravelling the regulatory structure of biochemical networks using stimulus response experiments and large-scale model selection. *IEE Systems Biology* Jul 2006; **153**(4):275–285.
15. Teusink B, Passarge J, Reijenga C, Esgalhado E, van der Weijden C, Schepper M, Walsh M, Bakker B, van Dam K, Westerhoff H, *et al.*. Can yeast glycolysis be understood in terms of in vitro kinetics of the constituent enzymes? Testing biochemistry. *European Journal of Biochemistry* Sep 2000; **267**(17):5313–5329.
16. Haunschild M, Freisleben B, Takors R, Wiechert W. Investigating the dynamic behavior of biochemical networks using model families. *Bioinformatics* Apr 2005; **21**(8):1617–1625.
17. Voit E, Alvarez-Vasquez F, Sims K. Analysis of dynamic labeling data. *Mathematical Biosciences* 2004; **191**(1):83–99.
18. Alvarez-Vasquez F, Hannun Y, Voit E. Dynamics of positional enrichment: Theoretical development and application to carbon labeling in *Zymomonas mobilis*. *Journal of Biochemical Engineering* 2008; **40**(1):157–174.
19. Wahl S, Nöh K, Wiechert W. ^{13}C labeling experiments at metabolic nonstationary conditions: An exploratory study. *BMC Bioinformatics* 2008; **9**(1):152.
20. Canelas A, Ras C, ten Pierick A, van Dam J, Heijnen J, van Gulik W. Leakage-free rapid quenching

technique for yeast metabolomics. *Metabolomics* 2008; **4**:226–239.
21. Canelas A, ten Pierick A, Ras C, Seifar R, van Dam J, van Gulik W, Heijnen J. Quantitative evaluation of intracellular metabolite extraction techniques for yeast metabolomics. *Analytical Chemistry* Sep 2009; **81**(17):7379–7389.
22. Büscher J, Czernik D, Ewald J, Sauer U, Zamboni N. Cross-platform comparison of methods for quantitative metabolomics of primary metabolism. *Analytical Chemistry* Mar 2009; **81**(6):2135–2143.
23. Seifar R, Zhao Z, van Dam J, van Winden W, van Gulik W, Heijnen J. Quantitative analysis of metabolites in complex biological samples using ion-pair reversed-phase liquid chromatography-isotope dilution tandem mass spectrometry. *Journal of Chromatography A* Apr 2008; **1187**(1-2):103–110.
24. de Jonge L, Buijs K, Heijnen J, van Gulik W, Wahl A. The dynamic metabolic response of *Penicillium chrysogenum* to feast/famine cycles. *Systems Biology of Microorganisms*, Paris, France, 2010.
25. Bemporad A, Morari M. Control of systems integrating logic, dynamics, and constraints. *Automatica* March 1999; **35**:407–427.
26. Sontag E. Nonlinear regulation: The piecewise linear approach. *IEEE Transactions on Automatic Control* 1981; **26**(2):346–358.
27. Heemels W, Schutter BD, Bemporad A. Equivalence of hybrid dynamical models. *Automatica* July 2001; **37**:1085–1091.
28. de Jong H. Modeling and simulation of genetic regulatory systems: A literature review. *Journal of Computational Biology* 2002; **9**(1):67–103.
29. Ghosh R, Amonlirdviman K, Tomlin C. A hybrid system model of planar cell polarity signaling in *Drosophila melanogaster* wing epithelium. *Proceedings of the 41st IEEE Conference on Decision and Control*, vol. 2, 2002; 1588–1594.
30. Batt G, Ropers D, de Jong H, Geiselmann J, Schneider D. Qualitative analysis and verification of hybrid models of genetic regulatory networks: Nutritional stress response in *Escherichia coli*. *in Hybrid Systems: Computation and Control*, Springer, 2005; 134–150.
31. Musters M, Lindenaar D, Juloski A, van Riel N. Hybrid identification of nonlinear biochemical processes. *14th IFAC Symposium on System Identification*, Newcastle, Australia, 2006.
32. Musters M, de Jong H, Van Den Bosch P, van Riel N. Qualitative analysis of nonlinear biochemical networks with piecewise-affine functions. *Hybrid Systems: Computation and Control*, *Lecture Notes in Computer Science*, vol. 4416, 2007; 727–730.
33. Lam C, Cross A. A systematic computerized method for building enzyme kinetic models. *Computers in Biology and Medicine* 1979; **9**(4):305–315.
34. Heijnen JJ. Approximative kinetic formats used in metabolic network modeling. *Biotechnology and Bioengineering* 2005; **91**(5):534–545.
35. Ferrari-Trecate G, Muselli M, Liberati D, Morari M. A clustering technique for the identification of piecewise affine and hybrid systems. *Automatica* 2003; **39**(2):205–217.
36. Bemporad A, Garulli A, Paoletti S, Vicino A. A bounded-error approach to piecewise affine system identification. *IEEE Transactions on Automatic Control* 2005; **50**(10):1567–1580.
37. Goel G, Chou I, Voit EO. System estimation from metabolic time-series data. *Bioinformatics* 2008; **24**(21):2505–2511.
38. Machina A, Ponosov A, Voit E. Automated piecewise power-law modeling of biological systems. *Journal of Biotechnology* 2010; **149**(3):154–165.
39. Kvasnica M, Grieder P, Baotić M. Multi-parametric toolbox (MPT) 2004. URL http://control.ee.ethz.ch/~mpt/.
40. Wiechert W, Möllney M, Petersen S, de Graaf A. A universal framework for ^{13}C metabolic flux analysis. *Metabolic Engineering* 2001; **3**(3):256–283.
41. Siuzdak G. *Mass spectrometry for biotechnology*. Boston: Academic Press, 1996.
42. Tyszka J, SE F, Jacobs R. Magnetic resonance microscopy: recent advances and applications. *Current Opinion in Biotechnology* 2005; **16**(1):93–99.
43. Habets L, Collins P, van Schuppen J. Reachability and control synthesis for piecewise-affine hybrid systems on simplices. *IEEE Transactions on Automatic Control* 2006; **51**:938–948.
44. Hamadeh A, Goncalves J. Reachability analysis of continuous-time piecewise affine systems. *Automatica* 2008; **44**(12):3189–3194.
45. Shawe-Taylor J, Cristianini N. *Kernel Methods for Pattern Analysis*. Cambridge University Press: New York, NY, USA, 2004.
46. Heinrich R, Schuster S. *The regulation of cellular systems*. Chapman & Hall, New York, 1996.
47. Paoletti S, Juloski A, Ferrari-Trecate G, Vidal R. Identification of hybrid systems - A tutorial. *European Journal of Control* 2007; **13**(2-3):242–260.
48. Juloski A, Heemels W, Ferrari-Trecate G, Vidal R, Paoletti S, Niessen J. Comparison of four procedures for the identification of hybrid systems. *Hybrid Systems: Computation and Control*, *Lecture Notes in Computer Science*, vol. 3414, 2005; 354–369.
49. Ferrari-Trecate G. Hybrid identification toolbox (HIT) 2005.
50. Roll J, Paoletti S. Piecewise affine identification toolbox (PWAid) 2007.
51. Ljung L. *System identification: Theory for the user*. Prentice-Hall, Englewood Cliffs, NJ, 1999.